The Rb isotope composition of modern seawater and outputs

1	The Rb isotope composition of modern seawater and outputs
2	to deep-sea sediments
3	Xingchao Zhang ^{1,2,8} , Limei Tang ³ , Jianghui Du ⁴ , Brian A. Haley ⁵ , James McManus ⁶ ,
4	Xia Hu², Fang Huang²,7*
5	
6	¹ Key Laboratory of Marine Geology and Metallogeny, First Institute of Oceanography,
7	MNR, Qingdao 266061, China
8	² CAS Key Laboratory of Crust–Mantle Materials and Environments, School of Earth
9	and Space Sciences, UST <u>C</u> , Hefei 230026, China
10	³ Key Laboratory of Submarine Geosciences, SOA, Second Institute of Oceanography,
11	MNR, China
12	⁴ School of Earth and Space Sciences, Peking University, Beijing 100871, China
13	⁵ College of Earth, Ocean and Atmospheric Sciences, Oregon State University,
14	Corvallis, OR, 97331, USA
15	⁶ Bigelow Laboratory for Ocean Sciences, East Boothbay, ME, USA
16	⁷ CAS Centre for Excellence in Comparative Planetology, USTC, Hefei 230026, China
17	⁸ Key Laboratory of Deep Sea Mineral Resources Development, Shandong
18	(preparatory), Qingdao 266061, China
19	
20	*Corresponding authors: fhuang@ustc.edu.cn (F. Huang)
21	Abstract: 285 words
22	Text: 5655 words
23	Figure: 6
24	Table: 0 (All in SI)
25	References: 72
26	Supplementary: 2 (1 text + 4 tables)

Abstract: The rubidium (Rb) isotope system has the potential for tracing water–silicate interactions and providing information on the global Rb cycling. However, the Rb isotope compositions of modern seawater and its major inputs and outputs remain poorly understood. Here we measured Rb isotope compositions of seawaters, pelagic clay sediments and porewaters from the western and central equatorial Pacific Ocean. Our results show that the δ^{87} Rb of modern seawater is homogeneous $(0.13 \pm 0.04\%)$; 2SD, n = 13) and higher than both the local sediments (-0.17‰ to 0.03‰) and the bulk lithosphere (Δ^{87} Rb_{seawater-UCC} = 0.27‰). The Rb in pelagic clay sediments is primarily associated with silicates (> 90%) and partially with exchangeable fractions (~ 4%). The exchangeable fractions display relatively lower δ^{87} Rb (-0.07 ± 0.05%; 2SD, n = 6). Meanwhile, the correlation between K/Rb and δ^{87} Rb of bulk sediments, along with investigations on the clay sized particles (δ^{87} Rb = -0.06‰), suggests that lithogenic silicates have relatively low K/Rb and δ⁸⁷Rb close to the UCC while formation of authigenic phillipsite or clays can result in higher bulk K/Rb (up to 930) and δ^{87} Rb (up to 0.03‰). However, the δ^{87} Rb of both authigenic silicates and absorbed fractions in deep-sea sediments are lower than seawater, which can partially contribute to the removal of isotopically light Rb and the heavy Rb isotope signal of the modern ocean. The δ^{87} Rb of the measured marine porewaters are approximately homogeneous (0.08%) to 0.14‰) and similar to seawater. The result consistent with previous K isotope investigation in this region that limited authigenic silicates were observed. Using a mass balance estimation in a steady state with isotope data, the flux of sediment removal for Rb in the ocean is about $2.2 - 12.0 \times 10^7$ kg/year.

Keywords: Rubidium isotopes, modern seawater, pelagic sediment, porewater

1. Introduction

Rubidium (Rb) is a lithophile element and highly enriched in the upper continental crust (UCC) relative to the mantle due to its high incompatibility (Rudnick and Gao, 2014). This element is primarily hosted by silicate minerals and is both fluid-mobile and significantly modified by secondary clays during chemical weathering (Nesbitt and Markovics, 1980; Teppen and Miller, 2006). In the modern ocean, Rb acts as a conservative alkali metal (e.g., Bruland et al., 2014). The variations of Rb concentrations and its ratios with other elements (e.g., K/Rb) in seawater and sediments generally reflect the impacts of silicate weathering and reverse weathering, as well as hydrothermal fluid interactions on Rb distributions (e.g., Edmond et al., 1979; Bayon et al., 2022; Li et al., 2022). Therefore, similar to isotope systems of other alkali metals (i.e., Li and K), Rb isotopes could potentially trace the impacts of silicate-water interactions. The development of Rb isotope analytical methods provides the possibility for new perspectives in understanding Rb cycling (Hu et al., 2021; Nebel et al., 2005; Nie and Dauphas, 2019; Pringle and Moynier, 2017; Zhang et al., 2018, 2023). Rubidium has two main isotopes, ⁸⁵Rb (72.17%) and ⁸⁷Rb (27.83%). ⁸⁷Rb decays to ⁸⁷Sr with a half-life of 4.97 × 10¹⁰ years, and thus ⁸⁷Rb/⁸⁵Rb can be regarded as a stable isotopic system (Nebel et al., 2011). A delta notion (δ^{87} Rb) is used to describe Rb isotope composition, defined as $[(^{87}\text{Rb}/^{85}\text{Rb})_{\text{sample}}/(^{87}\text{Rb}/^{85}\text{Rb})_{\text{SRM984}} - 1] \times 1000 (\%)$. Recent studies on soils and terrestrial sediments demonstrated that Rb isotopes can be a promising tracer of continental weathering (Hu et al., 2022; Zhang et al., 2021). However, our knowledge on Rb isotope variations in modern seawater and its major sources and sinks are currently limited, which hinders our mechanistic understanding of the source-to-sink transport of Rb.

The only reported seawater δ^{87} Rb value of the IAPSO reference from the North Atlantic (0.14 ± 0.13‰; Zhang et al., 2023) is higher than that of the UCC (-0.14 ± 0.01‰; Hu et al., 2022) and the bulk silicate Earth (BSE, -0.13 ± 0.06‰; Wang et al., 2023). Previous work showed that isotopically heavier Rb is preferentially retained by clays in soils with δ^{87} Rb from -0.30‰ to 0.08‰, leaving lower δ^{87} Rb values (mean value -0.22‰) in stream waters than the weathering products (Zhang et al., 2021). The results imply that riverine input alone is unlikely to produce the high δ^{87} Rb in seawater (Zhang et al., 2021). Further investigation on marine sediments and hydrothermal systems is necessary to resolve the origin of the seawater δ^{87} Rb signal.

Here we present Rb isotope data of seawaters, sediments, and porewaters from the Pacific Ocean, to constrain the δ^{87} Rb variations in the modern ocean and understand the potential impacts of sediment formation. Our results give an average δ^{87} Rb for seawater higher than that of the lithosphere, which could partially result from silicate authigenesis and absorption in deep—sea sediments.

2. Sample descriptions

Surface seawaters (within 100 m of the surface layer) were collected from the west Philippine basin and along the Kyushu–Palau ridge in the Western Pacific Ocean during DY68 cruise (Fig. 1; Table S1). Samples were collected using Niskin bottles and

passing through 0.45 μ m filters to acquire the dissolved pool. The filtered samples were acidic (pH ~ 2) and preserved in pre–cleaned PFA bottles. The study area was divided into two zones at 20°N based on differences in the water masses and temperature profile (Wang et al., 2023). Thus, these seawater samples can help understand the homogeneity of Rb isotope compositions at a regional scale. Combining with seawater standards (IAPSO, Nass-7 and Cass-6) from the North Atlantic, we could further constrain the Rb isotopic variations on a global scale.

The oxic sediments constitute a major part of modern seafloor, and recent investigations suggested that early diagenesis within pelagic sediments could play an important role in oceanic alkali metal cycling (e.g., Steiner et al., 2022). Sediments were collected from the Clarion-Clipperton Fe-Mn Nodule Zone using the Chinese manned submersible Jiao-long during DY125-31 cruise (Wu et al., 2019), and from the Pigafetta Basin by gravity piston-core during DY67 cruise of the research vessel "Xiangyanghong01". Samples were from stations of Dive64 (-154.29°E, 10.00°N), W1302 (-154.00°E, 10.07°N) and W1306 (-152.96°E, 6.75°N) at the central equatorial Pacific Ocean, as well as station of GC06 (152.18°E, 19.20°N) at the Western Pacific Ocean (Fig. 1; Table S2). All samples were from the abyssal plain (water depth > 4000) m). At each site, upper sediments were obtained (< 30 cm) to evaluate the potential influence of sediment formation on Rb. Samples studied here are brown and darkbrown pelagic clay sediments. Relatively higher contents of Fe–Mn (micro–) nodules were observed in samples Dive64–01 and Dive64–05. The station GC06 is located in REY-rich mud region, where abundant phillipsite can be observed (e.g., Shi et al., 2021; Li et al., 2023). Two samples with typically high phillipsite contents (high K/Rb) from deeper depth were also measured for a comparison (Table S2). These samples can help evaluate the impacts of different authigenic components.

Porewaters were collected at the central equatorial Pacific Ocean during KM2012 H101 cruise, with detailed methods described in Abbott et al. (2015) (Fig. 1; Table S3). In brief, sediment cores were collected using a multi-corer, and were visually inspected to be intact. Sediment intervals were transferred into centrifuge tubes and centrifuged at 10,000–12,000 rpm for 15 min. Porewater was acquired by taking the solution on the top of each tube and filtered by a 0.45µm membrane. Samples were from two distinct deep sea floor depositional settings: a red clay site (Station 3; -152°E, 11°N) and a carbonate rich site (Station 4; -152°E, 3°N). This study focuses on porewaters near the seawater–sediment interface (<10 cm). A previous K isotope study of these sediments (< 50 cm) revealed terrestrial illite as main K carrier (~ 90%), with the K isotope compositions similar to the UCC (Li et al., 2022). Rubidium isotope investigation of porewater can provide further understanding on the impacts of early diagenesis in deep–sea sediments.

3. Analytical methods

Isotope analyses were performed at the University of Science and Technology of China (USTC), China. The leaching experiments and mineralogical investigations were carried out at both the USTC and the First Institute of Oceanography, Ministry of Natural Resources (FIO), China. The major elemental compositions of the sediments

collected during DY125-31 and GC06 cruises have been measured at ALS Chemex (Guangzhou) Co., Ltd. (http://www.alsglobal.net.cn/) and the FIO by XRF, and the Rb contents of porewaters have been determined at the ETH Zurich by HR–ICP–MS (Element 2, Thermo–Fisher).

3.1. Sample digestion and mineralogical investigations

The sample evaporation and digestion procedure for seawater and porewater was modified from Zhang et al. (2023). In brief, 2.5 mL of each seawater sample with approximately 0.3 µg Rb were transferred into PFA beakers (Savillex) and evaporated at 100°C. To reach the volume of 2.5 mL, porewaters from several depths were mixed, with each depth contributes around 0.5–0.7 mL (Table S3). After evaporation, 1 mL concentrated nitric acid was added and heated overnight to digest residual organic matter. The samples were then evaporated and re-dissolved in 1mL 1.5 mol/L HCl for Rb purification and isotope analysis.

For sediments, approximately 30 mg bulk–sample powders were digested using first a mixture of concentrated HF–HNO₃ (~3:1, v/v) at 140 °C for 72 h in PFA beakers, and then a mixture of concentrated HCl–HNO₃ (~3:1, v/v) at 110 °C. After complete digestion, each solution was evaporated at 120 °C, followed by adding 1mL 1.5 mol/L HCl for Rb purification and isotope analysis.

Meanwhile, to better emphasize the potential impacts of authigenic silicates, sediment samples were immersed in deionized water for 24 h, and then the clay sized particles ($< 2 \mu m$) were obtained according to Stock's law determinations, following

the method described in Hu et al. (2023). The newly formed authigenic silicates would be less crystalized and can be more concentrated in clay sized fractions. Meanwhile, coarse fractions (> 63 μm) were obtained by wet sieved in 200 mesh sieves and coarse phillipsites were subsequently hand–picked under optical microscope. The collected clay sized particles and phillipsites were digested, along with elemental and isotopic analysis, following steps of bulk samples. Detail information is available in the SI.

3.2. Sequential extraction

Sequential extraction was carried out on W1302 and GC06 samples with steps modified from Tessier et al. (1979) and Rahman et al. (2017). More information is available in SI, with main steps summarized as follows:

- (1) Samples were rinsed with Milli–Q water for three times;
- (2) The exchangeable fraction was extracted using 1 mol/L ammonium acetate buffering solution (pH \sim 8) at 25 °C for 1 h. The pH was set to be close to the modern seawater, and the exchangeable fractions are interpreted to represent only parts of the elements adsorbed by the sediments;
 - (3) The reactive Si fraction was extracted by 4 mol/L NaOH at 60 °C for 2 h. This fraction is suggested to contain biogenic siliceous debris and parts of easily modified (authigenic) silicates, which is important regarding to authigenic silicate formation.
 - (4) The weak acid dissolvable fraction was leached by 1 mol/L ammonium acetate buffering solution (pH \sim 5) at 25 °C for 48 h. This step was previously conducted to extract carbonates. However, our samples were located below the CCD, and thus may

only potentially contain some bioapatite fossil (e.g., Liao et al., 2022);

- (5) The Fe–Mn hydroxide fraction was leached by 0.02 mol/L hydroxylammonium hydrochloride in 25% (v/v) acetate acid under 95 °C for 6 h;
- (6) The oxidizable fraction was extracted by 30% H_2O_2 in 0.02 mol/L HNO₃ (pH adjusted to \sim 2) under 85 °C for 6 h. This fraction is suggested to contain organic matter, whose concentration is very low in our samples.
- (7) The leaching residual was converted into PFA beakers and digested following steps of bulk sediments. The residual fraction contains mainly silicates, potentially including those from authigenic origins.

All leaching experiments were carried out at a solution/sample ratio of 10 mL / 100 mg. Leachates were separated by centrifuging at a rate of 5000 rpm for 5 min. All leachates and digested residuals were transferred to PFA beakers, evaporated at 100 °C, and then dissolved with 1 mL concentrated nitric acid. After that, 100 uL of leachates and 10 uL of leaching residuals were taken and diluted to 5 mL by 2% HNO₃ (m/m) for elemental concentration analysis. The remaining solutions were evaporated and redissolved in 1 mL 1.5 mol/L HCl for Rb purification and isotope analysis.

3.3. Concentration analyses

Major and trace elemental concentrations were analyzed by ICP–OES (iCAP6300, Thermo Fisher) and ICP–MS (Elan DRC, PerkinElmer; iCAP RQ, Thermo Fisher), respectively. The drift of the instrument over time was calibrated by using 10ppb Rh as an internal standard (Hou and Wang, 2007). The USGS standard BCR–2 was analyzed

using the same procedure, and the result agrees with literature data (Table S2; information available at GeoReM: http://georem.mpch-mainz.gwdg.de; Jochum et al., 2005). The uncertainties (RSD) of concentration data acquired are better than 5% for most of elements.

3.4. Rb purification and isotope composition analyses

Chromatographic purification of Rb for sediment samples completely follow the procedures established by Hu et al. (2021). It began first using Bio–Rad 200–400 mesh AG50W–X12 cation resin with 1.5 mol/L HCl and 1.5 mol/L HCl + 0.5 mol/L HF. This column chemistry was conducted twice for each sample. After this initial separation, samples were evaporated and dissolved in 3 mol/L HNO3 and Rb was further purified with Bio–Rad 50–100 mesh Sr–spec resin. The Rb leakage was monitored by measuring 1 mL aliquot before and after the "Rb–cut" using ICP–MS. Whole procedural blanks were less than 1 ng, which is negligible relative to the amount of Rb loaded on the column $(0.5-1~\mu g)$.

Several modifications have been made on column chemistry for seawater and porewater samples (Please see SI for more information). The elusion curve of Rb for seawater in AG50W–X12 cation resin could expand forward for at most 5 mL (Fig. S1a). Thus, 5 mL aliquots were additionally collected before the "Rb–cut" set in Hu et al. (2021). This will collect much more K than the previous procedure. Therefore, two more times purifications with Sr–spec resin were conducted to fully eliminate K. The Na/Rb, K/Rb, Ca/Rb, Mg/Rb and Sr/Rb ratios after the updated five–step procedure

 were all lower than 1 (Fig. S1c), leaving limited influences on Rb isotope analysis (Hu et al., 2021).

Rb isotope ratios were determined by MC–ICP–MS (Neptune Plus, Thermo Fisher) in low resolution mode, using sample–standard bracketing calibration method described in Hu et al. (2021). NIST SRM984 was used as the "zero–delta" standard during the measurement, with final results reported in delta notion: δ^{87} Rb = $[(^{87}\text{Rb}/^{85}\text{Rb})_{\text{sample}}/(^{87}\text{Rb}/^{85}\text{Rb})_{\text{SRM984}}-1] \times 1000\%$. ⁸⁸Sr was measured to calibrate the isobaric interference of ⁸⁷Sr on ⁸⁷Rb, with ⁸⁷Sr/⁸⁸Sr ratio of 0.085. The signals of ⁸⁸Sr after purification are generally less than 1 mV during measurement, thus having a negligible influence on the results.

The external reproducibility of $\delta^{87}Rb$ measurements at the USTC was assessed based on long–term analyses on in–house standard ICP–Rb and USTC–Rb for over one year, which is -0.31 \pm 0.05‰ (2SD, n = 276) and -0.15 \pm 0.03‰ (2SD, n = 78), respectively. The measured $\delta^{87}Rb$ in this study was -0.31 \pm 0.05‰ (2SD, n = 10) for ICP–Rb, -0.15 \pm 0.03‰ (2SD, n = 10) for USTC–Rb and -0.14 \pm 0.01‰ (2SD, n = 3) for BCR–2, in agreement with literature data (Hu et al., 2021; Zhang et al., 2023). Meanwhile, five independent IAPSO seawater standard measurements were performed and display a mean $\delta^{87}Rb$ at 0.13 \pm 0.05‰ (2SD, n = 5), which is also consistent with literature data (Zhang et al., 2023) and could represent the external reproducibility of seawater analysis (Fig. S1d; Table S1). The whole procedural replicates agreed within analytical uncertainty (Table S1 and S2). Rb concentrations were calculated through signal comparison with 100 ppb NIST SRM 984. The Rb content calculated was 48

ppm for BCR-2 and 1.44 µmol/L for IAPSO, consistent with literature data (Table S1 and S2; information available at GeoReM: http://georem.mpch-mainz.gwdg.de; Jochum et al., 2005).

4. Results

The elemental and Rb isotope compositions of seawater, sediment and porewater samples are shown in Table S1 to Table S3, respectively. Results of leaching experiments are in Table S4.

4.1. Water samples

The 10 seawater samples from the Western Pacific Ocean have $\delta^{87}Rb$ varying from 0.09‰ to 0.16‰, with mean value at 0.13 ± 0.04‰ (2SD, n = 10) (Fig. 2; Table S1). The Rb concentrations of these samples range from 1.27 µmol/L to 1.54 µmol/L. No significant spatial variations can be identified (Table S1). Similar $\delta^{87}Rb$ were observed for the three seawater standards (IAPSO, Nass-7 and Cass-6) from the North Atlantic Ocean, with $\delta^{87}Rb$ at 0.13‰, 0.12‰ and 0.12‰, respectively (Table S1).

The δ^{87} Rb of porewaters from Station 3 and 4 in the central equatorial Pacific Ocean are similar to each other and to the modern seawater, with isotope and elemental compositions varying from 0.08‰ to 0.14‰ (n = 4) and 1.50 µmol/L to 1.63 µmol/L, respectively (Fig. 2; Table S3).

4.2. Bulk sediments, minerals and leachates of sequential extraction

Samples Dive64–01 and Dive64–05 have much higher Mn and Fe concentrations due to abundant Fe-Mn (micro–) nodules, with relatively low Rb contents (Table S2). However, similar δ^{87} Rb ranges have been observed among the four sediment profiles (Fig. 3 and S2). Taken together, the δ^{87} Rb of pelagic clay sediments range from -0.17‰ to 0.03‰, with mean value at -0.09 \pm 0.13‰ (2SD, n = 20). The δ^{87} Rb are within that of the UCC and the modern seawater (Fig. 3). The clay sized particles display δ^{87} Rb at -0.06‰ with relatively high K/Rb at around 640, while much higher K/Rb was observed for phillipsite at around 1530 (Fig. 3; Table S2).

Leaching experiments indicate that ~ 90% of Rb is in refractory silicates, and ~ 4% is in the exchangeable fraction (Table S4). The Rb proportions in reactive Si fractions decrease sharply with increasing depth (Fig. 4c). The δ^{87} Rb of residuum post-leaching (-0.17‰ to 0.01‰; Table S4) were comparable to bulk compositions (Δ^{87} Rb_{residual-bulk} = -0.02‰ to 0.03‰; Fig. 4a, b). In contrast, the exchangeable fractions have relatively homogeneous δ^{87} Rb (-0.11‰ to -0.04‰) even though the bulk compositions have varied significantly (Fig. 4a, b; Table S4). The mean δ^{87} Rb of the exchangeable fractions is -0.07 ± 0.05‰ (2SD, n = 6), which is around 0.20‰ lower than that of the modern seawater (Fig. 4a, b).

5. Discussion

5.1. The Rb isotope composition of modern seawater

Homogeneous δ^{87} Rb (0.09‰ to 0.16‰, mean value at 0.13‰) were observed in seawater samples from the Western Pacific Ocean (Fig. 2). Similar δ^{87} Rb were also

 observed for IAPSO, Nass-7 and Cass-6 seawater references from the North Atlantic (mean δ^{87} Rb at 0.12%; Table S1), supporting the notion of a homogeneous δ^{87} Rb for the modern ocean. The mean Rb concentration in seawater globally is around 1.4 μmol/kg (Bruland et al., 2014), and the total ocean mass is about 1.35×10²¹ kg (Baumgartner and Reichel, 1975), thus the total amount of Rb dissolved in seawater is 1.6×10¹⁴ kg. As the major inputs of Rb into ocean, the annual riverine flux of Rb is 3.2 -6.1×10^7 kg, while annual hydrothermal input flux is $2.2 - 8.1 \times 10^7$ kg (Berner and Berner, 2012; Elderfield and Schultz, 1996; Gaillardet et al., 2014; Hart and Staudigel, 1982; Staudigel, 2014; Wheat et al., 2017). Based on these estimates, the residence time of Rb calculated here is around 1.1 - 3.0 million years, within the range of previous work (e.g., 0.6 - 3.4 million years; Bolter et al., 1964; Edmond et al., 1979), which is much longer than the average mixing time of seawater (about 2000 years). Therefore, although detailed spatial and depth distributions are not addressed by our samples, the conservative distribution of Rb in the modern ocean allows us to anticipate a homogenous average Rb isotope composition of δ^{87} Rb = 0.13 ± 0.04‰ (2SD, n = 13). The δ^{87} Rb of modern seawater is about 0.27% higher than that of the UCC (-0.14 \pm 0.01‰; Hu et al., 2022) and the BSE (-0.13 \pm 0.06‰; Wang et al., 2023). To understand the differences between seawater and lithosphere, we need to make quantitative constraints on the primary inputs and outputs of Rb to the oceans, including riverine and hydrothermal inputs, as well as any isotopic fractionations during marine sediment formation and oceanic crust alteration (e.g., Berner and Berner, 2012; Wang et al., 2021). To our knowledge, no Rb isotope data has been reported to date for these

inputs and outputs. Based on investigations in a granite weathering profile, the heavy Rb isotope is preferentially retained in soils, which would result in a lower δ^{87} Rb in river water (Zhang et al., 2021). Indeed, the mean δ^{87} Rb of stream water is -0.22‰, but this is much lower than seawater (Zhang et al., 2021). Therefore, riverine input cannot readily explain the δ^{87} Rb difference between seawater and lithosphere. Assuming no isotope fractionation during high temperature hydrothermal alteration on oceanic crust, hydrothermal fluid likely has relatively low δ^{87} Rb, given the light Rb isotope composition of middle ocean ridge basalt (-0.13‰; Nie and Dauphas, 2019; Wang et al., 2023; Zhang et al., 2023). Other potential interpretations for the seawater δ^{87} Rb include interactions following a sediment sink and/or crustal alteration, which is also proposed for Li and K isotope investigations (e.g., Penniston-Dorland et al., 2017; Wang et al., 2021).

5.2. Deep-sea sediment as an isotopically light sink for Rb

5.2.1 Potential impacts of silicate authigenesis

Our results show a δ^{87} Rb variation from -0.17‰ to 0.03‰ in pelagic clay sediments, generally lower than the modern seawater value (Fig. 3). The variations of δ^{87} Rb in bulk sediments are predominantly controlled by silicate minerals (> 90% total sediment Rb; Table S4). Previous works suggested that lithogenic clays, primarily sourced from Asian or American dust, constitute the major part of pelagic clay sediments (e.g., Jones et al., 1994; Nakai et al., 1993; Uematsu et al., 1983). However, recent investigations revealed that there could be significant clay authigenesis in pelagic

 red clay sediments (Steiner et al., 2022), and abundant authigenic smectite and zeolite (phillipsite) formed in deep—sea REY—rich muds (e.g., Li et al., 2023; Wang et al., 2024). The silicate—water interactions in deep—sea sediments could have important influences on global oceanic elemental budgets (e.g., Baldermann et al., 2015; März et al., 2015; Steiner et al., 2023). Here, potential impacts of authigenic phillipsite and clays on Rb cycling are discussed.

Phillipsite is a common authigenic silicate mineral in pelagic sediments and can be formed by low–temperature alteration of volcanic materials (Hay and Shappard, 2001). Coarse phillipsite were identified under microscope for samples from GC06 station (Fig. S3), which show an enrichment in K with much higher K/Rb (\sim 1500). The preference of K by phillipsite has been reported in previous investigations (e.g., Hay and Sheppard, 2001; Li et al., 2023). The δ^{87} Rb of GC06 samples shifted from a crustal value (δ^{87} Rb \sim -0.15‰, K/Rb \sim 487) to compositions with much higher δ^{87} Rb (-0.04‰ to 0.03‰) and K/Rb (\sim 900), indicating that phillipsite formation results in higher bulk δ^{87} Rb (Fig. 3a). The δ^{87} Rb is still lower than the seawater, suggesting phillipsite can be an isotopically light sink of Rb in the ocean.

Meanwhile, processes forming authigenic clay in deep–sea sediments include recrystallization of detrital aluminosilicates and/or alteration of biogenic silica (Steiner et al., 2022). Compared to Chinese loess that is representative of the Asian dust and usually the UCC (-0.17‰ to -0.07‰; Hu et al., 2022), four samples from W1302, W1306 and Dive64 stations display typically higher δ^{87} Rb (-0.03‰ to 0.03‰) with relatively high K/Rb (~ 570) (Fig. 3a). Interestingly, the leaching experiments showed

that relatively higher Rb proportions in reactive Si fractions were observed for both surface sediment and also sample W1302-4 with a high bulk δ^{87} Rb of 0.03‰ (Fig. 4a, c). The high value of surface sediment was due to high content of biogenic siliceous debris (Fig. S3), which dissolved in the deeper part (e.g., Rahman et al., 2017; Steiner et al., 2022). While the higher Rb proportion in the reactive Si fraction of sample W1302-4 would imply more reactive (authigenic) silicates (Rahman et al., 2017). Similarly higher δ^{87} Rb (-0.06‰) and K/Rb (~640) were observed in clay sized particles that potentially contain authigenic silicates (Fig. 3a). Previous observations also suggest that due to the high K/Rb of the seawater, authigenic silicates precipitated from it tend to have higher K/Rb with variable isotope compositions (e.g., Hu et al., 2020; Li et al., 2022). Thus, the relatively higher δ^{87} Rb and K/Rb in these samples would imply potential impacts of clay authigenesis, which are still lower than the seawater and can potentially be an isotopically light sink of oceanic Rb cycling.

5.2.2 Potential impacts from other processes

Absorption–driven Rb isotope fractionation may not be important for bulk sediment compositions (~ 4% total sediment Rb; Table S4), but fractionation can influence the composition of porewater and seawater, which has been suggested in a K isotope study (Santiago Ramos et al., 2018). The exchangeable fractions in our leaching experiment display homogeneous δ^{87} Rb with a mean value at -0.07 \pm 0.05‰ (2SD, n = 6), even though the samples are from different regions and bulk δ^{87} Rb have changed significantly (Fig. 4a, b). A possible explanation would be that the variations of bulk

 compositions were mainly driven by the extent of silicate authigenesis, while exchangeable fractions may continue to undergo ion exchange with the surrounding waters, representing re-equilibrium of the absorbed Rb with surrounding waters. The Δ^{87} Rb_{exchangeable-seawater} is approximately -0.20‰, implying a preferential adsorption of light Rb isotope by sediments. This observation is consistent with a laboratory absorption experiment that Rb⁺ forms inner–sphere complexes in phyllosilicates (i.e., vermiculite and illite) with negative Δ^{87} Rb_{solid-liquid} (Konagaya et al., 2022).

Fe–Mn hydroxides are also important authigenic phases in deep–sea sediment, but they are less significant for sequestering Rb (<1% total sediment Rb; Table S4). The phase is represented by Dive64–01 and –05 samples, which are enriched in Fe–Mn (micro–) nodules and have lower Rb/Ti and similar bulk δ^{87} Rb compared to other samples (Table S2; Fig. 4b). Thus, an abundance of Fe–Mn hydroxides could result in dilution of the total sedimentary Rb content, but have limited impacts on bulk δ^{87} Rb.

Here, a homogenous δ^{87} Rb is observed in porewaters in surface sediments (upper 10 cm) at the central equatorial Pacific Ocean (Fig. 2; Table S3). In this region, the K isotope compositions of bulk sediment are similar to that of the UCC, suggesting limited impact of early diagenesis (Li et al., 2023). Meanwhile, despite the presence of phillipsite in the upper sediment layers at station GC06 (Fig. S1), the δ^{87} Rb of the bulk samples are close to that of the UCC (Fig. 3). To produce a detectable change in δ^{87} Rb (i.e., at least 0.05% that is the long-term analytical uncertainty), the modified fraction of Rb in bulk sediments can be simply calculated as $f_{\text{modified}} = 0.05\%$ / ($\delta_{\text{modified}} - \delta_{\text{initial}}$), where the δ_{modified} is assumed to be 0.03% and the δ_{modified} is -0.14%. Thus, over 30%

of Rb is need to be authigenic to significantly change the bulk δ^{87} Rb. Considering the relatively high Rb contents in porewaters (~1.6 μ mol/L) and sediments (~80ppm), δ^{87} Rb similar to seawater or the UCC would be observed if the extent of water-silicate interaction is relatively low.

5.3. The Rb budgets of the modern ocean

Here we review the flux data of major inputs (rivers and hydrothermal fluids) and outputs (sediments and oceanic crust alteration) for Rb in the modern ocean, and constrain the elemental mass balance with isotope data (Fig. 5). At a steady state, the elemental and isotopic fluxes into the ocean are equal to the output fluxes:

$$F_{riv} + F_{hyd} = F_{sed} + F_{alt}$$
 (Eq. 1)

 $F_{nv} \times \delta^{87} Rb_{nv} + F_{hyd} \times \delta^{87} Rb_{hyd} =$

416
$$F_{sed} \times (\delta^{87}Rb_{sw} + \Delta^{87}Rb_{sed}) + F_{alt} \times (\delta^{87}Rb_{sw} + \Delta^{87}Rb_{alt}) \quad (Eq. 2)$$

Where the F_{riv} , F_{hyd} , F_{sed} , and F_{alt} represent the fluxes (kg/year) of Rb from riverine (riv) and hydrothermal (hyd) inputs, Rb outputs to marine authigenic/adsorbed sediments (sed), and altered oceanic crust (alt), respectively. The $\delta^{87}Rb_{sw}$, $\delta^{87}Rb_{riv}$, and $\delta^{87}Rb_{hyd}$ represent Rb isotope compositions of seawater, river water, and hydrothermal fluid, respectively. $\Delta^{87}Rb_{sed}$ and $\Delta^{87}Rb_{alt}$ represent Rb isotope fractionation during sediment formation and crustal alteration.

The estimations in previous studies of F_{riv} and F_{hyd} are $3.2 - 6.1 \times 10^7$ kg/year and

 2.2 – 8.1×10⁷ kg/year, respectively (Fig. 5; Hart and Staudigel, 1982; Elderfield and Schultz, 1996; Berner and Berner, 2012; Gaillardet et al., 2014; Staudigel, 2014; Wheat et al., 2017); while F_{alt} is around $1.6 - 3.2 \times 10^7$ kg/year (Fig. 6; Elderfield and Schultz, 1996; Hart and Staudigel, 1982; Staudigel, 2014; Staudigel et al., 1996). Because it is difficult to directly estimate F_{sed} for whole ocean Rb due to variability in lithogenic phases (e.g., Thomson et al., 1984), a variation of $0.0 - 20.0 \times 10^7$ kg/year was assumed for F_{sed} for initial Monte Carlo simulations (please see SI for more information). Only limited information available for δ^{87} Rb of major inputs and outputs. We assume that the extent of equilibrium K isotope fractionation is around 3.5 times that of Rb (Zeng et al., 2019). As the Rb isotope fractionation in continental margin sediments are currently unknown, the Δ^{87} Rb_{sed} is inferred to vary between -0.41% to -0.04‰, according to the Δ^{41} K_{sed} from -1.42‰ to -0.14‰ observed in sediments (Hu et al., 2020; Li et al., 2022). The Δ^{41} K_{alt} is from -0.88% to 0.04% based on data of altered oceanic crust (Hu et al., 2020; Liu et al., 2021; Liu et al., 2023; Parendo et al., 2017; Santiago Ramos et al., 2020), implying a Δ^{87} Rb_{alt} from -0.25% to 0.01%. Since δ^{87} Rb_{riv} and δ^{87} Rb_{hyd} are not known, we assume that δ^{87} Rb_{riv} has a range from -0.37% to -0.07%, which is the mean δ^{87} Rb of stream water $\pm 0.15\%$ (Zhang et al., 2021). While δ^{87} Rb_{hyd} was assumed to vary between compositions of seawater and the BSE (-0.13% to 0.13%); Wang et al., 2023; This study). Combining these assumptions with the δ^{87} Rb_{sw} observed, ten billion Monte Carlo simulations were performed to refine the data. The result indicates a F_{sed} at $2.2 - 12.0 \times 10^7$ kg/year (Fig. 5). The variation of F_{sed} is largely driven by F_{hvd} (Fig. S4a). Meanwhile, the uncertainty of $\Delta^{87}Rb_{sed}$ also displays relatively

significant influence on the flux estimation (Fig. S4b). Based on current data, the proportion of sediment removal in total Rb output fluxes is around 40 – 85%, suggesting sediments as a major sink of Rb in the ocean (Fig. S4). Further Rb elemental and isotopic investigations on major inputs and outputs will improve the constrains on oceanic Rb budgets.

Here, potential impact of groundwater was not assessed due to data limitations. Nevertheless, previous investigations suggested that the contribution of groundwater on Li budgets would be 5% - 43% that of riverine input with similar isotope composition (Mayfield et al., 2021). If we assume that groundwater provides a Rb flux that is also 5% - 43% to the riverine Rb input, it won't result in magnitude changes in our mass balance estimations. Meanwhile, the observed δ^{87} Rb of authigenic silicates and absorbed fractions in deep—sea sediments (-0.07‰ to 0.03‰) are currently higher than the candidates of riverine (stream water: -0.22‰) and hydrothermal (the BSE: -0.13‰) inputs. To achieve a mass balance in the oceanic Rb cycling, identification of isotopically lighter sinks or heavier sources is necessary. A wider range of δ^{41} K was observed in continental margin sediments and altered crusts with relatively high K/Rb (e.g., Hu et al., 2020; Li et al., 2022). Further Rb isotope investigations in these areas would help find the missing isotopically light Rb sink in the ocean.

5.4. A comparison with other alkali and alkaline earth elements

Most of the alkali and alkaline earth elements are conservative in the ocean with residence times at several million years (i.e., 0.8 – 10.1 Ma for Li, K, Ca, Mg, Sr;

 Lecuyer et al., 2016). Their isotopic budgets in the ocean hold promise as tracers of long-term tectonic/climatic forcing on ocean chemistry. In general, the isotope compositions of these elements in seawater are all heavier than the riverine input, and most of them (i.e., Li, K, Ca, Sr) in rivers are also heavier than the lithosphere, except Rb and Mg (Fig. 6; Gussone et al., 2016; Paytan et al., 2021; Penniston-Dorland et al., 2017; Teng, 2017; Wang et al., 2021). The preferential release of heavy isotopes during silicate weathering and the removal of light isotopes by carbonate burial contribute to the higher dissolved $\delta^{44/42}$ Ca and $\delta^{88/86}$ Sr in rivers and seawater (e.g., Krabbenhoft et al., 2010; Blättler et al., 2012). Meanwhile, the enrichment of light isotopes by clays during incongruent continental weathering and silicate authigenesis also results in the elevated dissolved δ^7 Li and δ^{41} K in rivers and the ocean (e.g., Penniston-Dorland et al., 2017; Wang et al., 2021). In contrast, lower δ^{87} Rb and δ^{26} Mg are observed in stream/river waters, due to the preferential retention of heavy isotopes by secondary clays, and significant release of isotopically light Mg during carbonate weathering (e.g., Tipper et al., 2006; Zhang et al., 2021). Furthermore, the higher δ^{87} Rb_{sw} and δ^{26} Mg_{sw} than riverine inputs suggest an overall preferential removal of light isotopes during oceanic processes (e.g., Li et al., 2015; Shavel et al., 2019). Based on the information, distinct evolution curves and controlling factors for seawater isotope compositions can be expected. Ambiguity remains when evaluating the relative impacts of continental weathering and seafloor interactions on ocean chemistry (e.g., Coogan and Dosso, 2022). For example, the rise of δ⁷Li_{SW} in Cenozoic seawater can result from enhanced incongruent

continental weathering, changes in the rate of clay formation, and/or slowdown of seafloor spreading (e.g., Misra and Froelich, 2012; Caves Rugenstein et al., 2019; Coogan and Dosso, 2022; Zhang et al., 2022; Cai et al., 2024). Deciphering the specific contributions from these processes is challenging due to their similar isotope variation tendencies. Rb isotopes generally display fractionations opposite to Li during continental weathering, but behave similarly during oceanic processes (Fig. 6). Therefore, the similarity or difference between the δ^7 Lisw and δ^{87} Rbsw evolution curves can potentially help constrain the relative importance of oceanic processes versus continental weathering in changing seawater chemistry.

6. Conclusions

This study reports Rb isotope compositions in modern surface seawaters, porewaters and deep—sea sediments. Major conclusions are summarized as follows:

- (1) Modern seawater has a homogeneous δ^{87} Rb with mean value at $0.13 \pm 0.04\%$ (2SD, n = 13). This value is around 0.27% higher than that of the lithosphere.
- (2) The correlation between bulk K/Rb and δ^{87} Rb (-0.17‰ to 0.03‰) of sediments, along with leaching experiments and mineralogical investigations, suggest that silicate authigenesis (clay and phillipsite) and absorption in deep—sea sediments contribute to removal of isotopically light Rb from seawater, and partially result in the high δ^{87} Rb in the ocean.
- (3) A Monte Carlo simulation based on Rb isotope mass balance model indicates that Rb fluxes of sediment removal is at $2.2 12.0 \times 10^7$ kg/year. However, isotopically

lighter sinks of Rb than the sediments observed in this study are still required to reach the mass balance of oceanic Rb cycling.

(4) Our data generally suggest that oceanic outputs would drive the $\delta^{87}Rb$ of seawater to higher values, contrasting previous investigations in a soil profile that incongruent continental weathering tends to produce lower $\delta^{87}Rb$ in rivers and subsequently in seawater. Such opposite variation tendencies of Rb isotopes are different from those observed for Li and K and can potentially provide new constrains on the evolution of ocean chemistry.

Acknowledgements

This project was financed by the National Natural Science Foundation of China (42330101). The pore water sampling cruise was funded by US NSF grant 1850765 to Brian Haley and 1850789 to James McManus. We would thank the captain and crew of the R/V Kilo Moana for making the cruise possible at the height of the COVID pandemic. We would also thank Xuefa Shi and the captain and crew of the R/V Xiangyanghong01 for collecting the REY-rich sediments. Meanwhile, we would thank Huimin Yu and Yaqi Zhang for the help of Rb isotope analyses and Zhenhui Hou for the help of elemental concentration analyses at the USTC.

532	References
533	Abbott, A. N., Haley, B. A., McManus, J. 2015. Bottoms up: Sedimentary control of
534	the deep North Pacific Ocean's εNd signature. Geology 43(11), 1035-1035.
535	Baldermann, A., Warr, L. N., Letofsky-Papst, I., Mavromatis, V. 2015. Substantial iron
536	sequestration during green-clay authigenesis in modern deep-sea sediments. Nat
537	Geosci. 8(11), 885–889
538	Baumgartner, A., Reichel, E., Lee R., 1975. The World Water Balance: Mean Annual
539	Global, Continental and Maritime Precipitation, Evaporation and Run-off.
540	Elsevier Scientific Publishing Company.
541	Bayon, G., Bindeman, I.N., Trinquier, A., Retallack, G.J., Bekker, A., 2022. Long-term
542	evolution of terrestrial weathering and its link to Earth's oxygenation. Earth
543	Planet. Sci. Lett. 584.
544	Berner, K., Berner, R. A., 2012. Global Environment: Water, Air, and Geochemical
545	Cycles. Princeton University Press, Princeton, New Jersey.
546	Blättler, C.L., Henderson, G.M., Jenkyns, H.C., 2012. Explaining the Phanerozoic Ca
547	isotope history of seawater. Geology 40(9), 843-846.
548	Bolter, E., Turekian, K.K., Schutz D.F., 1964. The Distribution of Rubidium, Cesium
549	and Barium in the Oceans. Geochim. Cosmochim. Acta. 28, 1459–1466.
550	Bruland, K.W., Lohan, M.C., Middag, R.H., 2014. Controls of trace metals in seawater.
551	In Treatise on Geochemistry (eds. H. D. Holland and K. K. Turekian), 2nd ed.
552	Elsevier, Oxford, pp. 19–51.

Cai, D., Shao, H., Gou, L.F., Jin, Z.D., Z., Yang, S., 2024. Lithium isotope fractionation

- during submarine hydrothermal alteration processes. Geochimica et Cosmochimica Acta, 371, 65-77. Caves Rugenstein, J.K., Ibarra, D.E., von Blanckenburg, F., 2019. Neogene cooling driven by land surface reactivity rather than increased weathering fluxes. *Nature* 571(7763), 99-102. Coogan, L.A., Dosso, S.E., 2022. Controls on the evolution of Cenozoic seawater chemistry. Geochim. Cosmochim. Acta. 329, 22-37. Edmond, J.M., Measures, C., McDuff, R.E., Chan, L.H., Collier, R., Grant, B., 1979. Ridge crest hydrothermal activity and the balances of the major and minor elements in the ocean: The Galapagos data. Earth Planet. Sci. Lett. 46, 1–18. Elderfield, H., Schultz, A., 1996. Mid-ocean ridge hydrothermal fluxes and the chemical composition of the ocean. Annu. Rev. Earth Planet. Sci. 24, 191–224. Gaillardet, J., Viers, J., Dupré, B., 2014. Trace Elements in River Waters. In *Treatise on* Geochemistry (eds. H. D. Holland and K. K. Turekian), 2nd ed. Elsevier, Oxford, pp. 195-235. Gussone, N., Schmitt, A.-D., Heuser, A., Wombacher, F., Dietzel, M., Tipper, E., Schiller, M., Bohm, F., 2016. Calcium stable isotope geochemistry. Springer. Hart, S.R., Staudigel, H., 1982. The control of alkalies an uranium in seawater by ocean crust alteration. Earth Planet. Sci. Lett. 58, 202-212. Hay, R. L., and Sheppard, R. A., 2001. Occurrence of zeolites in sedimentary rocks: An
- Hou, Z.H., Wang, C.X., 2007. Determination of 35 trace elements in geological samples

overview. Rev. Mineral Geochem. 45(1), 217-234.

by inductively coupled plasma mass spectrometry. J. Uiv. Sci. Tech. China 37, 940-944. Hu, Q., Yang, B., Liu, J., Li, B., Dang, Y., Zhu, A., Zhang, P., Chen, J., Li, C., Song, Z., Shi, X. 2023. Geochemical and mineral composition characteristics of hydrothermal-related clay-sized surface sediments from southern Mid-Atlantic Ridge: implications for hydrothermal depositional environment. Ore Geol. Rev. 105674. Hu, X., Nan, X., Liu, X., Huang, F., 2022. Rubidium isotope compositions of the average upper continental crust and the Himalayan leucogranites: Implications for magmatic-fluid interaction. Geochim. Cosmochim. Acta 336, 165–176. Hu, X., Nan, X.Y., Yu, H.M., Huang, F., 2021. High precision Rb isotope measurements by MC-ICP-MS. J. Anal. At. Spectrom. 36, 2744–2755. Hu, Y., Teng, F.-Z., Plank, T., Chauvel, C., 2020. Potassium isotopic heterogeneity in subducting oceanic plates. Sci. Adv. 6, eabb2472. Jochum, K. P., Nohl, U., Herwig, K., Lammel, E., Stoll, B., Hofmann, A. W., 2005. GeoReM: a new geochemical database for reference materials and isotopic standards. Geostand Geoanal Res. 29(3), 333-338. Jones, C.E., Halliday, A.N., Rea, D.K., Owen, R.M., 1994. Neodymium isotopic variations in North Pacific modern silicate sediment and the insignificance of detrital REE contributions to seawater. Earth Planet. Sci. Lett. 127, 55-66. Konagaya, R., Tsuboi, H., Itai, T., and Takahashi, Y., 2022. Selective isotope

fractionation of rubidium during adsorption on phyllosilicate minerals as a

- tracer of water-rock interaction. In 2022 Goldschmidt Conference. GOLDSCHMIDT. Krabbenhoft A., Eisenhauer A., Bo"hm F., Vollstaedt H., Fietzke J., Liebetrau V., Augustin N., Peucker-Ehrenbrink B., Muller M. N., Horn C., Hansen B. T., Nolte N., Wallmann K., 2010. Constraining the marine strontium budget with natural strontium isotope fractionations (87Sr/86Sr*, d88/86Sr) of carbonates, hydrothermal solutions and river waters. Geochim. Cosmochim. Acta 74, 4097-4109. Li, S., Fu, Y., Li, D., Huang, F., Sun, X. and He, G. 2023. Phillipsite in pelagic REYrich sediments and ferromanganese nodules from the Western Pacific: Geochemical characteristics and implications for REY enrichments. Ore Geol. Rev. 161, 105631. Li, W., Beard, B.L., Li, C., Xu, H., Johnson, C.M., 2015. Experimental calibration of Mg isotope fractionation between dolomite and aqueous solution and its geological implications. Geochim. Cosmochim. Acta 157, 164–181. Li, W.S., Liu, X.M., Wang, K., McManus, J., Haley, B.A., Takahashi, Y., Shakouri, M., Hu, Y., 2022. Potassium isotope signatures in modern marine sediments: Insights into early diagenesis. Earth Planet. Sci. Lett. 599, 117849. Liao, J., Chen, J., Sun, X., Wu, Z., Deng, Y., Shi, X., Wang, T., Chen, Y. and Koschinsky, A. 2022. Quantifying the controlling mineral phases of rare-earth elements in
 - Liu, H.Y., Xue, Y.Y., Zhang, G.L., Sun, W.D., Tian, Z., Tuller-Ross, B., Wang, K., 2021.

deep-sea pelagic sediments. Chem. Geol. 595, 120792.

Potassium isotopic composition of low-temperature altered oceanic crust and its impact on the global K cycle. Geochim. Cosmochim. Acta 311, 59-73. Liu, Y. D., Guo, Z., Tian, H. C., Qin, G., and Peng, X., 2023. Potassium isotopic fractionation during multistage alteration of oceanic crust in the southern Mariana Trench. Chem. Geol. 620, 121350. März, C., Meinhardt, A. K., Schnetger, B., Brumsack, H. J. 2015. Silica diagenesis and benthic fluxes in the Arctic Ocean. Mar. Chem. 171, 1–9. Mayfield, K. K., Eisenhauer, A., Santiago Ramos, D. P., Higgins, J. A., Horner, T. J., Auro, M., Magna, T., Moosdorf, N., Charette, M.A., Gonneea, M.E., Brady, C.E., Komar, N., Peucker-Ehrenbrink B., Paytan, A. 2021. Groundwater discharge impacts marine isotope budgets of Li, Mg, Ca, Sr, and Ba. Nat. Commun. 12(1), 148. Misra, S., Froelich, P.N., 2012. Lithium Isotope History of Cenozoic Seawater: Changes in Silicate Weathering and Reverse Weathering. Science 335(6070), 818-823. Nakai, S.I., Halliday, A.N., Rea, D.K., 1993. Provenance of dust in the Pacific Ocean. Earth Planet. Sci. Lett. 119, 143-157. Nebel, O., Mezger, K., Scherer, E.E., Münker, C., 2005. High precision determinations of 87Rb/85Rb in geologic materials by MC-ICP-MS. Int. J. Mass Spectrom. 246, 10–18.

Nebel, O., Scherer, E.E., Mezger, K., 2011. Evaluation of the 87Rb decay constant by

age comparison against the U-Pb system. Earth Planet. Sci. Lett. 301, 1–8.

pp. 1-51.

- Nesbitt, H.W., Markovics, G., 1980. Chemical processes affecting alkalis and alkaline earths during continental weathering. Geochim. Cosmochim. Acta 44(11), 1659-1666. Nie, N.X., Dauphas, N., 2019. Vapor drainage in the protolunar disk as the cause for the depletion in volatile elements of the moon. Astrophys. J. 884(2). Parendo, C.A., Jacobsen, S.B., Wang, K., 2017. K isotopes as a tracer of seafloor hydrothermal alteration. Proc. Natl. Acad. Sci. 114(8), 1827-1831. Paytan, A., Griffith, E.M., Eisenhauer, A., Hain, M.P., Wallmann, K., Ridgwell, A., 2021. A 35-million-year record of seawater stable Sr isotopes reveals a fluctuating global carbon cycle. Science 371(6536), 1346-1350. Penniston-Dorland, S., Liu, X.M., Rudnick, R.L., 2017. Lithium isotope geochemistry. Rev. Mineral Geochem. 82, 165–217. Pringle, E.A., Moynier, F., 2017. Rubidium isotopic composition of the Earth, meteorites, and the Moon: evidence for the origin of volatile loss during planetary accretion. Earth Planet. Sci. Lett. 473, 62–70. Rahman, S., Aller, R. C., Cochran, J. K., 2017. The missing silica sink: Revisiting the marine sedimentary Si cycle using cosmogenic 32Si. Global Biogeochem. Cy. 31(10), 1559-1578. Rudnick, R.L., Gao, S., 2014. Composition of the Continental Crust. In Treatise on Geochemistry (eds. H. D. Holland and K. K. Turekian), 2nd ed. Elsevier, Oxford,
- 663 Santiago Ramos, D.P., Coogan, L.A., Murphy, J.G., Higgins, J.A., 2020. Low-

temperature oceanic crust alteration and the isotopic budgets of potassium and magnesium in seawater. Earth Planet. Sci. Lett. 541. Santiago Ramos, D.P., Morgan, L.E., Lloyd, N.S., Higgins, J.A., 2018. Reverse weathering in marine sediments and the geochemical cycle of potassium in seawater: Insights from the K isotopic composition (41K/39K) of deep-sea pore fluids. Geochim. Cosmochim. Acta 236, 99-120. Shaley, N., Bontognali, T.R., Wheat, C.G., Vance, D., 2019. New isotope constraints on the Mg oceanic budget point to cryptic modern dolomite formation. Nat. Commun. 10(1), 5646. Shi, X., Bi, D., Huang, M., Yu, M., Luo, Y., Zhou, T., Zhang, Z., Liu, J., 2021. Distribution and metallogenesis of deep-sea rare earth elements. Geol. Bull. China 40 (2/3), 195–208 (in Chinese with English abstract). Staudigel, H., 2014. Chemical fluxes from hydrothermal alteration of the oceanic crust. In Treatise on Geochemistry (eds. H. D. Holland and K. K. Turekian), 2nd ed. Elsevier, Oxford, pp. 583–606. Staudigel, H., Plank, T., White, W.M., Schmincke, H.U., 1996. Geochemical fluxes during seafloor alteration of the basaltic upper oceanic crust: DSDP Sites 417 and 418. In: Bebout GE, Scholl DW, and Kirby SH (eds.) Subduction: Top to Bottom, Geophysical Monograph Series, vol. 96, pp. 19–38. Washington, DC: American Geophysical Union. Steiner, Z., Antler, G., Berelson, W. M., Crockford, P. W., Dunlea, A. G., Hou, Y.,

Adkins J. F., Turchyn, A. V. and Achterberg, E. P., 2023. Trace Element

Geochemistry in North Pacific Red Clay Sediment Porewaters and Implications for Water-Column Studies. Global Biogeochem. Cy. 37(11), e2023GB007844. Steiner, Z., Rae, J. W. B., Berelson, W. M., Adkins, J. F., Hou, Y., Dong, S., Lampronti, G. I., Liu, X., Achterberg, E. P., Subhas, A. V. and Turchyn, A. V., 2022. Authigenic formation of clay minerals in the abyssal North Pacific. Global Biogeochem. Cv. 36(11), e2021GB007270. Teng, F.-Z., 2017. Magnesium isotope geochemistry. Rev. Mineral Geochem. 82(1), 219-287. Teppen, B.J., Miller, D.M., 2006. Hydration energy determines isovalent cation exchange selectivity by clay minerals. Soil Sci. Soc. Am. J. 70(1), 31–40. Tessier, A.P.G.C., Campbell, P.G., Bisson, M.J.A.C., 1979. Sequential extraction procedure for the speciation of particulate trace metals. Anal. chem. 51(7), 844-851. Thomson, J., Carpenter, M.S.N., Colley, S., Wilson, T.R.S., Elderfield, H., Kennedy, H., 1984. Metal accumulation rates in northwest Atlantic pelagic sediments. Geochim. Cosmochim. Acta 48, 1935-1948. Tipper, E. T., Galy, A., Gaillardet, J., Bickle, M. J., Elderfield, H., Carder, E. A., 2006. The magnesium isotope budget of the modern ocean: constraints from riverine magnesium isotope ratios. Earth Planet. Sci. Lett. 250(1-2), 241-253. Uematsu, M., Duce, R.A., Prospero, J.M., Chen, L., Merrill, J.T., McDonald, R.L., 1983. Transport of mineral aerosol from Asia over the North Pacific Ocean. J.

Geophys. Res., Oceans 88(C9), 5343-5352.

- Wang, B., Dong, Y., Han, X., Li, X., Wang, Y., Zhang, W. and Chu, F. 2024. Enrichment
 of smectite in the REY-rich mud of the Clarion-Clipperton Fracture Zone in the
 eastern Pacific and its geological significance. *Geochem. Geophy. Geosy.* 25(2),
 e2023GC011283.
 Wang, B., Moynier, F., Jackson, M.G., Huang, F., Hu, X., Halldórsson, S.A., Dai, W.,
- Devos, G., 2023. Rubidium isotopic fractionation during magmatic processes and the composition of the bulk silicate Earth. *Geochim. Cosmochim. Acta* 354, 38-50.
- Wang, K., Li, W., Li, S., Tian, Z., Koefoed, P., Zheng, X.Y., 2021. Geochemistry and cosmochemistry of potassium stable isotopes. *Geochemistry* 125786.
- Wang, Z., Fang, C., Yang, C., Zhang, G., Sun, D. (2023). Latitudinal gradient and
 influencing factors of deep-sea particle export along the Kyushu-Palau Ridge in
 the Philippine Sea. Sci. Total Environ. 167460.
- Wheat, C. G., Fisher, A. T., McManus, J., Hulme, S. M., Orcutt, B. N. (2017). Cool
 seafloor hydrothermal springs reveal global geochemical fluxes. *Earth Planet*.
 Sci. Lett. 476, 179-188.
- Wu, F., Owens, J. D., Tang, L., Dong, Y., Huang, F., 2019. Vanadium isotopic
 fractionation during the formation of marine ferromanganese crusts and nodules.
 Geochim. Cosmochim. Acta 265, 371-385.
- Zeng, H., Rozsa, V. F., Nie, N. X., Zhang, Z., Pham, T. A., Galli, G., Dauphas, N., 2019.
 Ab initio calculation of equilibrium isotopic fractionations of potassium and
 rubidium in minerals and water. ACS Earth Sp. Chem. 3, 2601–2612.

Zhang, F., Dellinger, M., Hilton, R.G., Yu, J., Allen, M.B., Densmore, A.L., Sun, H., Jin, Z., 2022. Hydrological control of river and seawater lithium isotopes. Nat. Commun. 13(1). doi.org/10.1038/s41467-022-31076-y. Zhang, Z., Ma, J., Wang, Z., Zhang, L., He, X., Zhu, G., Zeng, T., Wei, G., 2021. Rubidium isotope fractionation during chemical weathering of granite. Geochim. Cosmochim. Acta 313, 99-115. Zhang, Z., Ma, J., Zhang, L., Liu, Y., Wei, G., 2018. Rubidium purification via a single chemical column and its isotope measurement on geological standard materials by MC-ICPMS. J. Anal. At. Spectrom. 33, 322-328. Zhang, Z., Ma, J., Zhang, L., Liu, Y., Wei, G., 2023. Rubidium Isotope Ratios of International Geological Reference Materials. Geostand Geoanal Res. 47(3), 697-712. Zheng, X.-Y., Beard, B.L., Neuman, M., Fahnestock, M.F., Bryce, J.G., Johnson, C.M., 2022. Stable potassium (K) isotope characteristics at mid-ocean ridge hydrothermal vents and its implications for the global K cycle. Earth Planet.

Sci. Lett. 593, 117653.

Figure captions

Fig. 1. Sample locations in this study including seawaters (DY68 cruise), porewaters

(KM2012 H101 cruise) and sediments (DY125-31 cruise and DY67 cruise). The

overview map was produced using Ocean Data View. Color bar on the right side

represents the water depth.

Fig. 2. The Rb isotope compositions of water samples. The blue and orange backgrounds represent the average δ^{87} Rb of seawater and the UCC, respectively. The UCC data are from Hu et al. (2022).

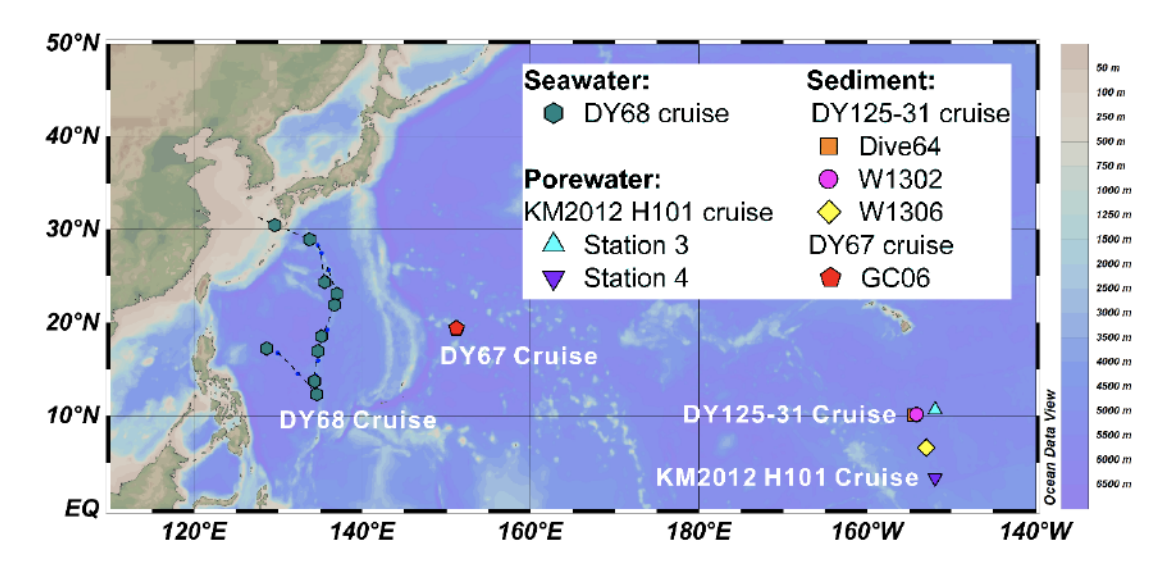
Fig. 3. Relationships between δ⁸⁷Rb and (a) molar K/Rb and (b) Rb/Ti for sediment samples. Literature data of loess, river sediments, sedimentary rocks and the UCC (orange pentagram) were plotted for a comparison, which are from Hu et al. (2022) and Rudnick and Gao (2014). The red arrow and purple arrow represent more contributions from phillipsite and Fe–Mn hydroxides, respectively. The green triangle represents the composition of clay sized particles.

 Fig. 4. Leaching experiment results for the δ^{87} Rb of (a) W1302 station and (b) GC06 station, and (c) Rb proportions in the reactive Si fractions. The blue and orange backgrounds represent the average compositions of seawater and the UCC, respectively. Data of the UCC are from Hu et al. (2022).

Fig. 5. Schematic diagrams illustrating the global ocean Rb isotopic mass balance. Flux estimates are in blue and are ×10⁷ kg/year. Mean concentrations of the UCC and modern seawater are in green. The δ^{87} Rb values are in red. Data shown here are seawater (Bruland et al., 2014; Zhang et al., 2023; This study), the UCC (Rudnick and Gao, 2014; Hu et al., 2022), riverine input (Hart and Staudigel, 1982; Elderfield and Schultz, 1996; Berner and Berner, 2012; Gaillardet et al., 2014; Zhang et al., 2021), hydrothermal input (Hart and Staudigel, 1982; Elderfield and Schultz, 1996; Berner and Berner, 2012; Staudigel, 2014; Wang et al., 2023), altered oceanic crust (Hart and Staudigel, 1982; Elderfield and Schultz, 1996; Staudigel et al., 1996; Staudigel, 2014) and sediment (though mass balance estimation; This study).

Fig. 6. A comparison of isotope compositions among the UCC, river water and modern seawater. Data shown here are $\delta^7 \text{Li}$ (Penniston-Dorland et al., 2017; and references therein), $\delta^{41} \text{K}$ (Wang et al., 2021; and references therein), $\delta^{87} \text{Rb}$ (Hu et al., 2022; Zhang et al., 2021; This study), $\delta^{26} \text{Mg}$ (Teng, 2017; and references therein), $\delta^{44/42} \text{Ca}$ (Gussone et al., 2016; and references therein), and $\delta^{88/86} \text{Sr}$ (Pearce et al., 2015; and references therein). The dash line represents the 1:1 line, implying same compositions between water and the UCC.

791 Figures



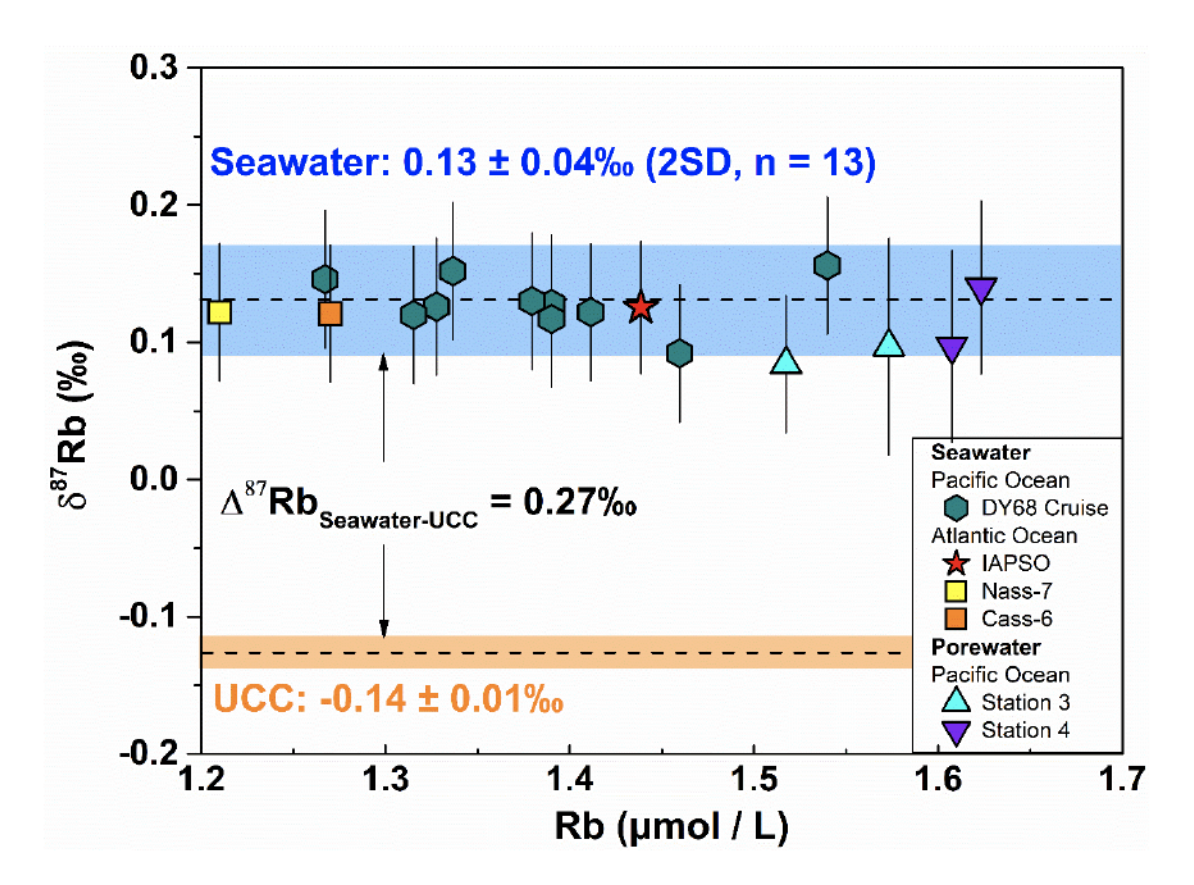
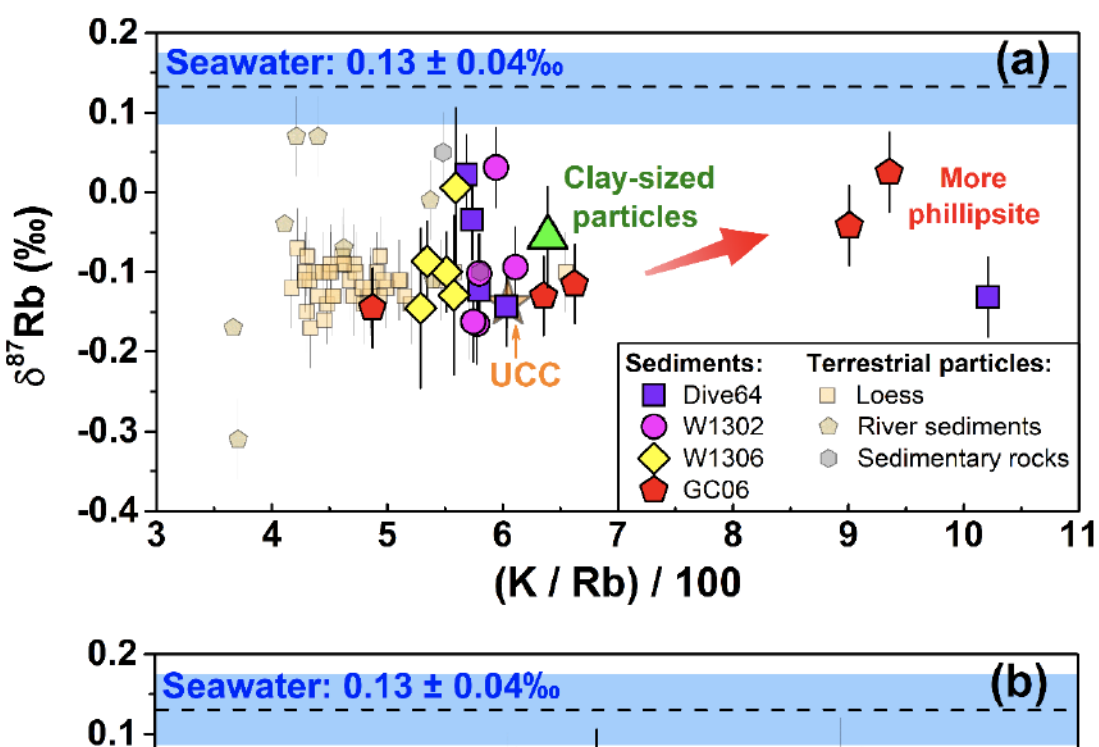
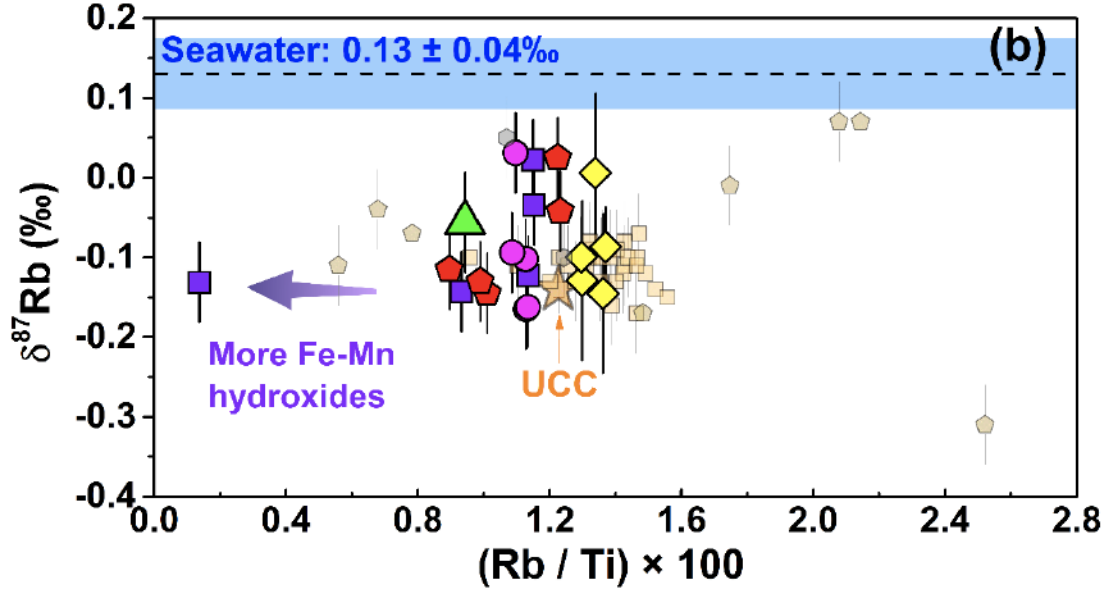
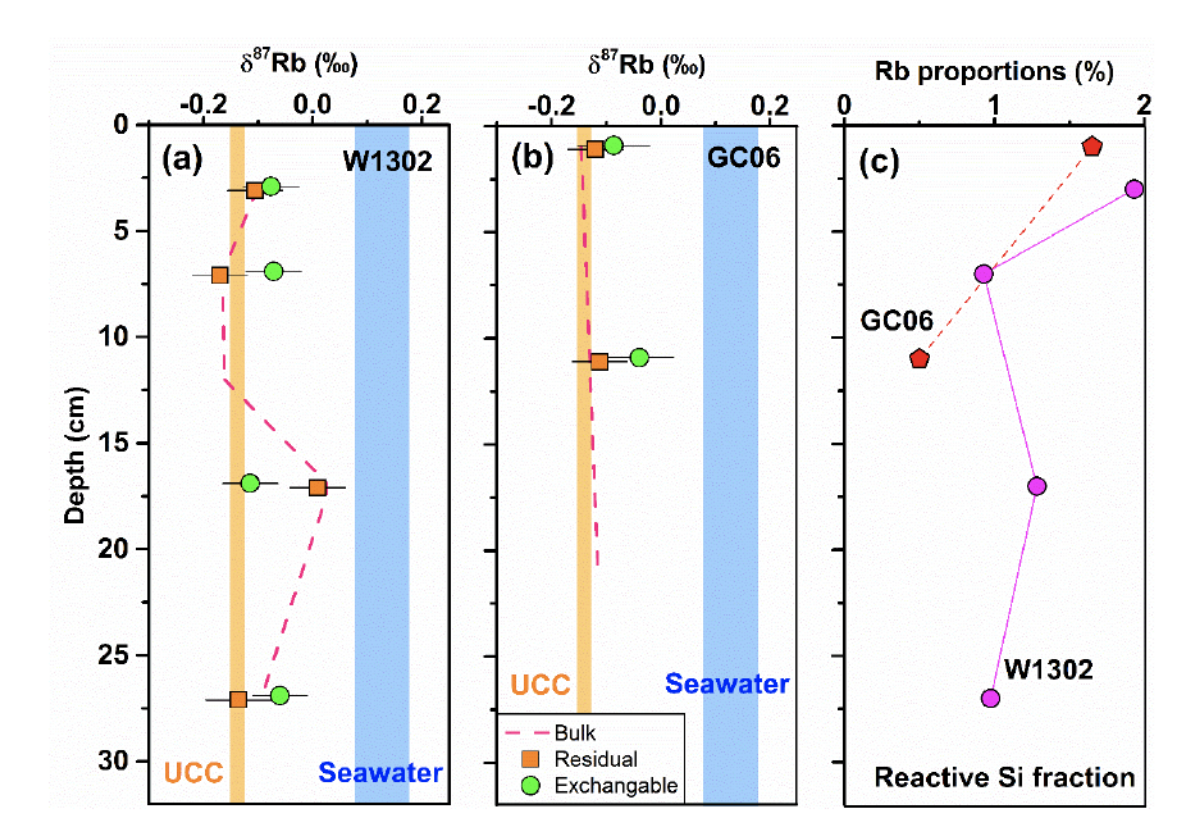
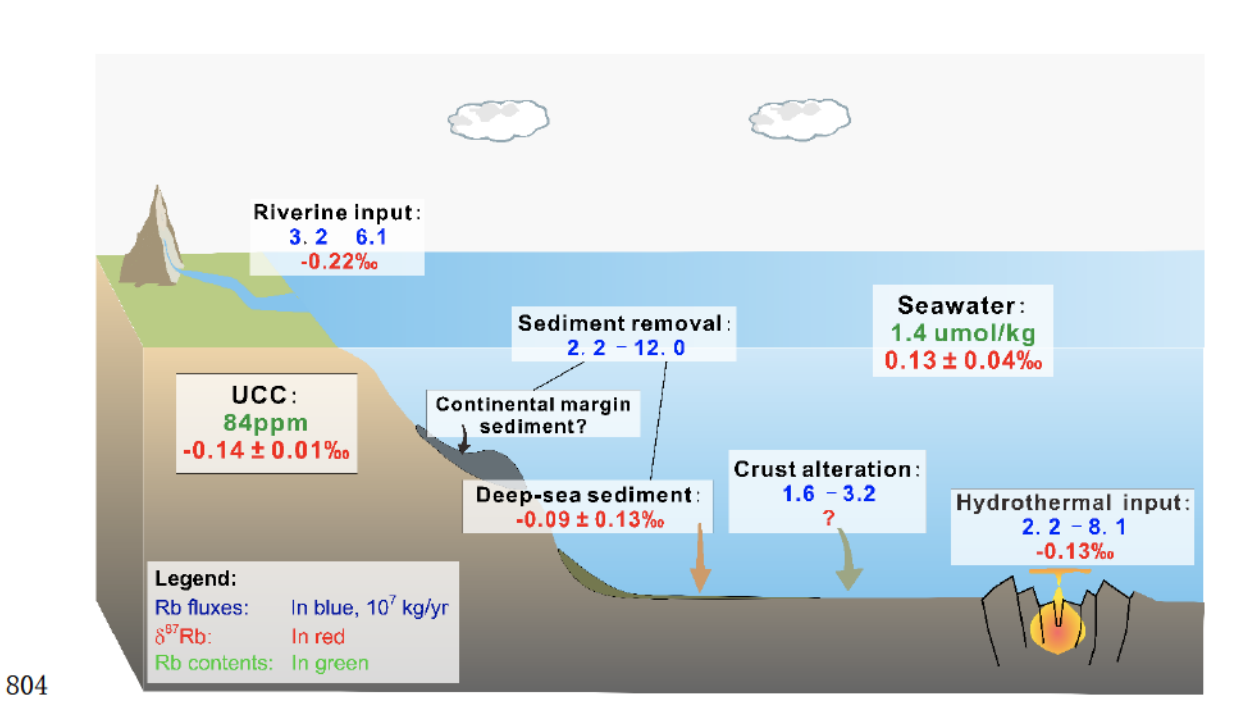


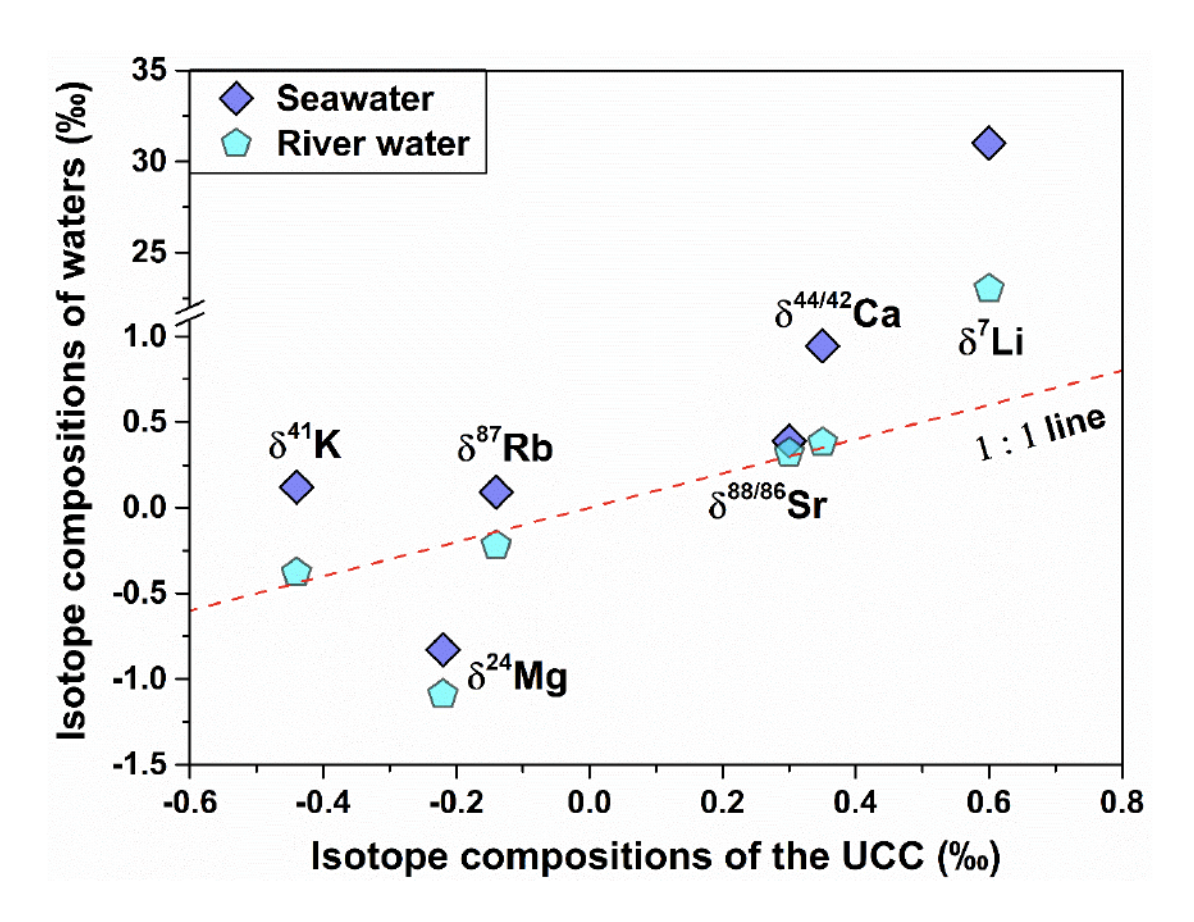
Fig. 2











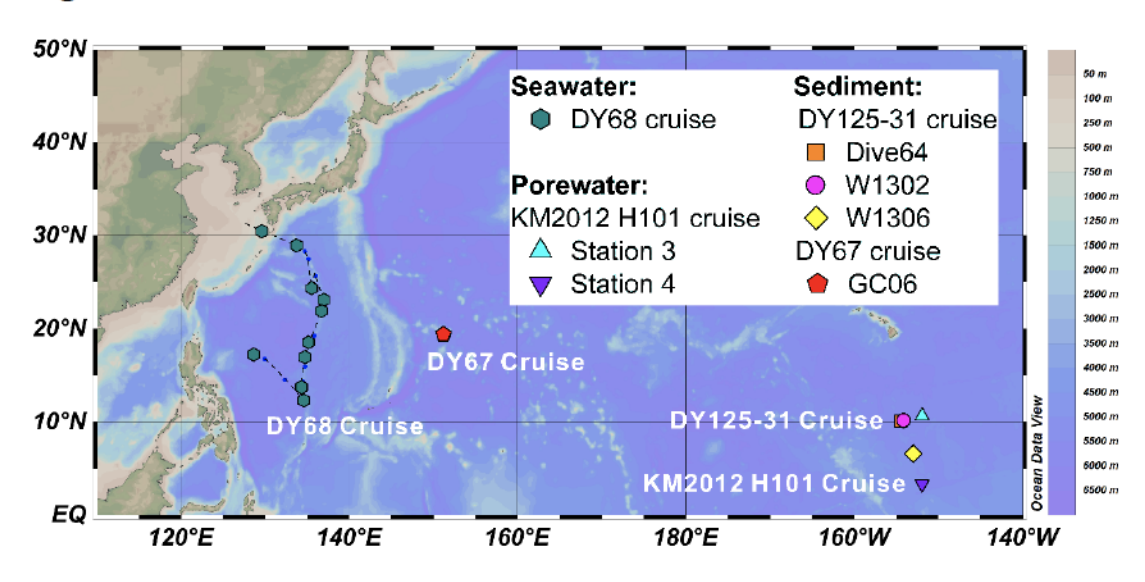
Figures

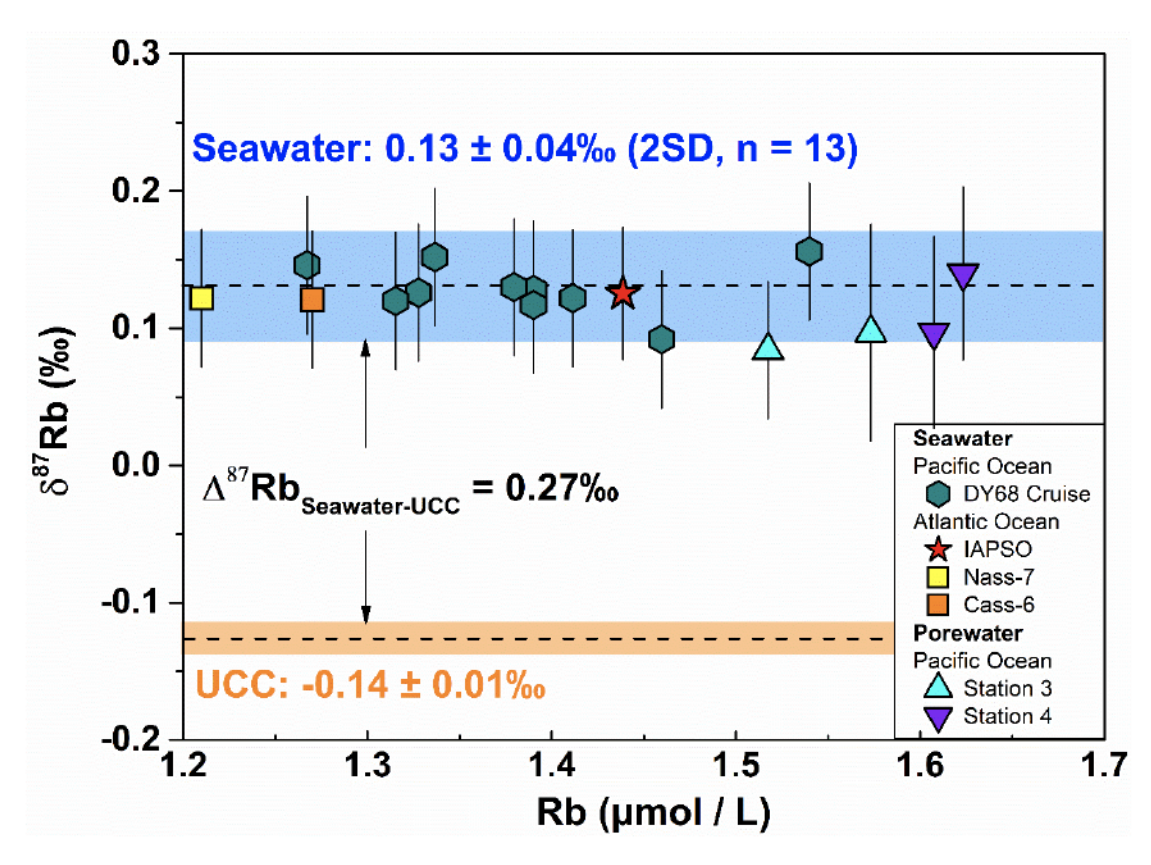
1

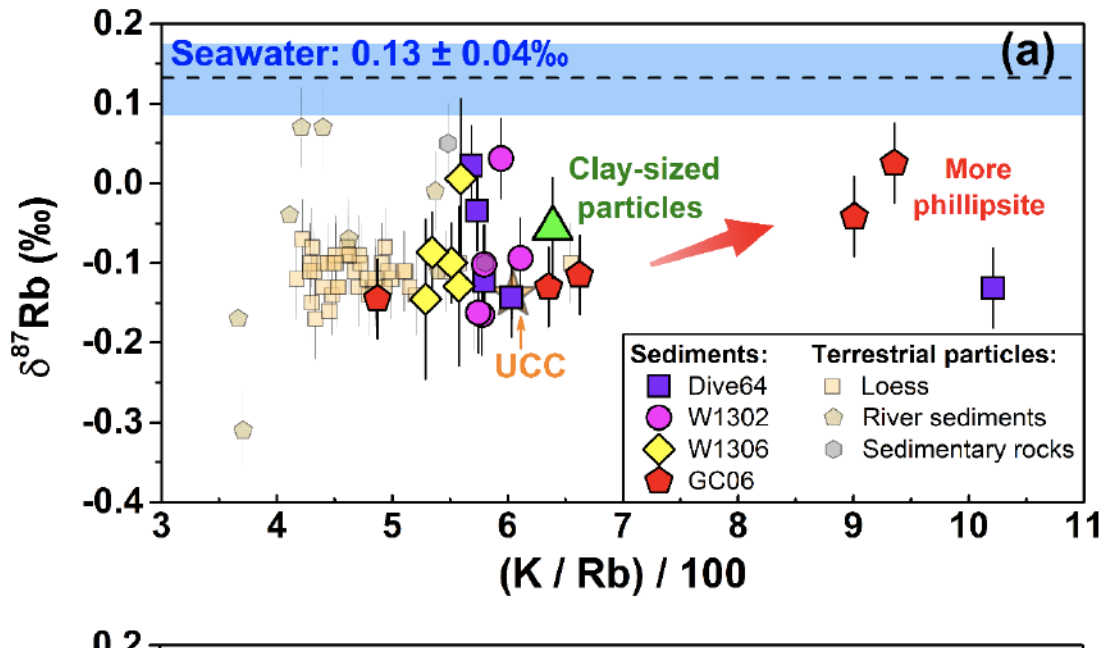
2

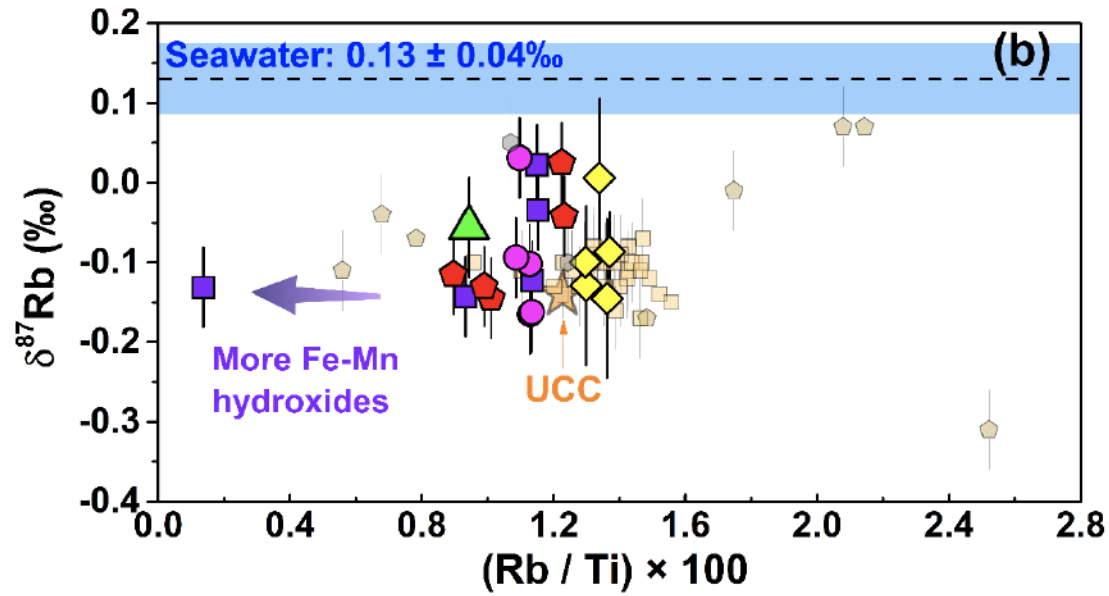
3

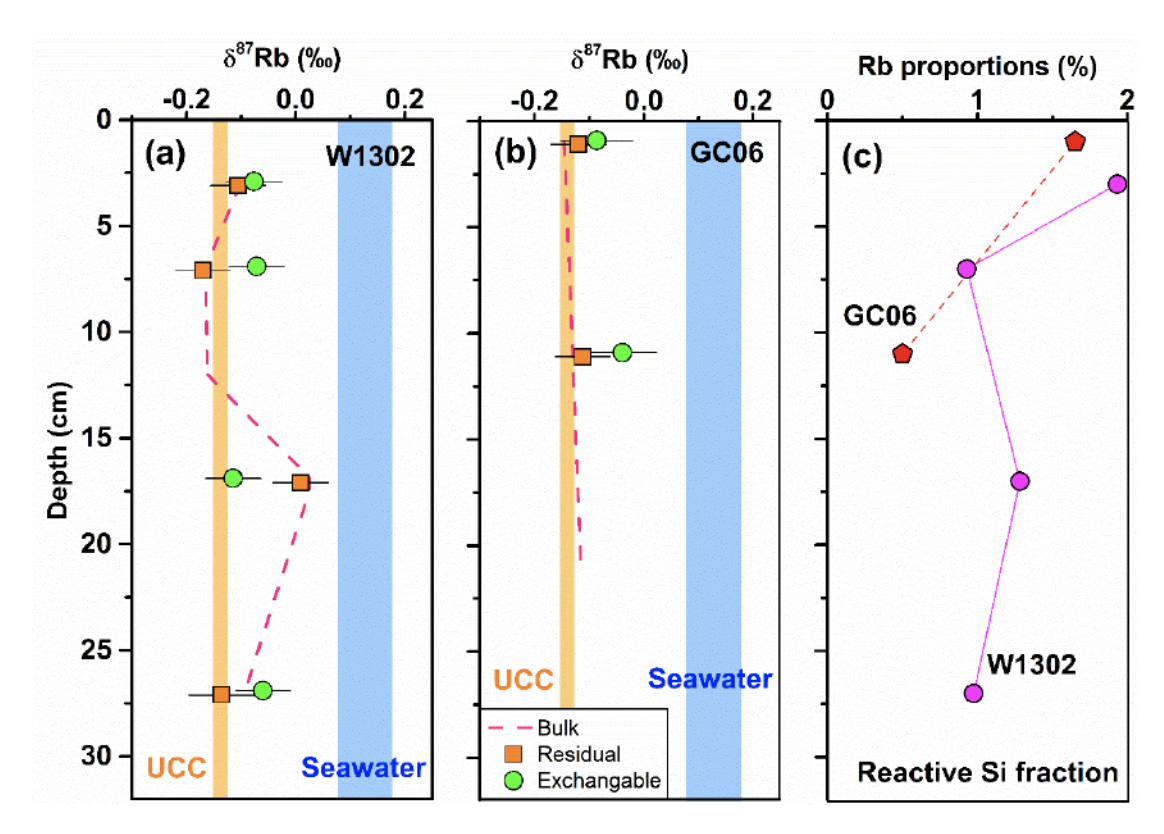
4

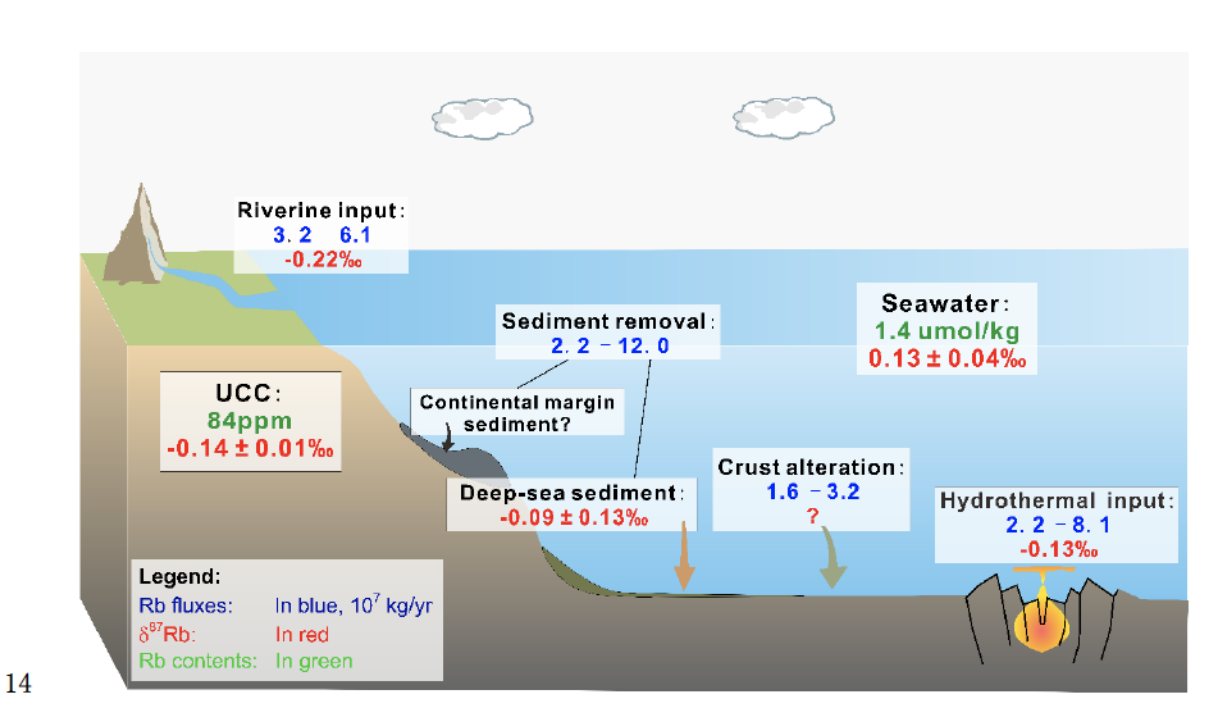


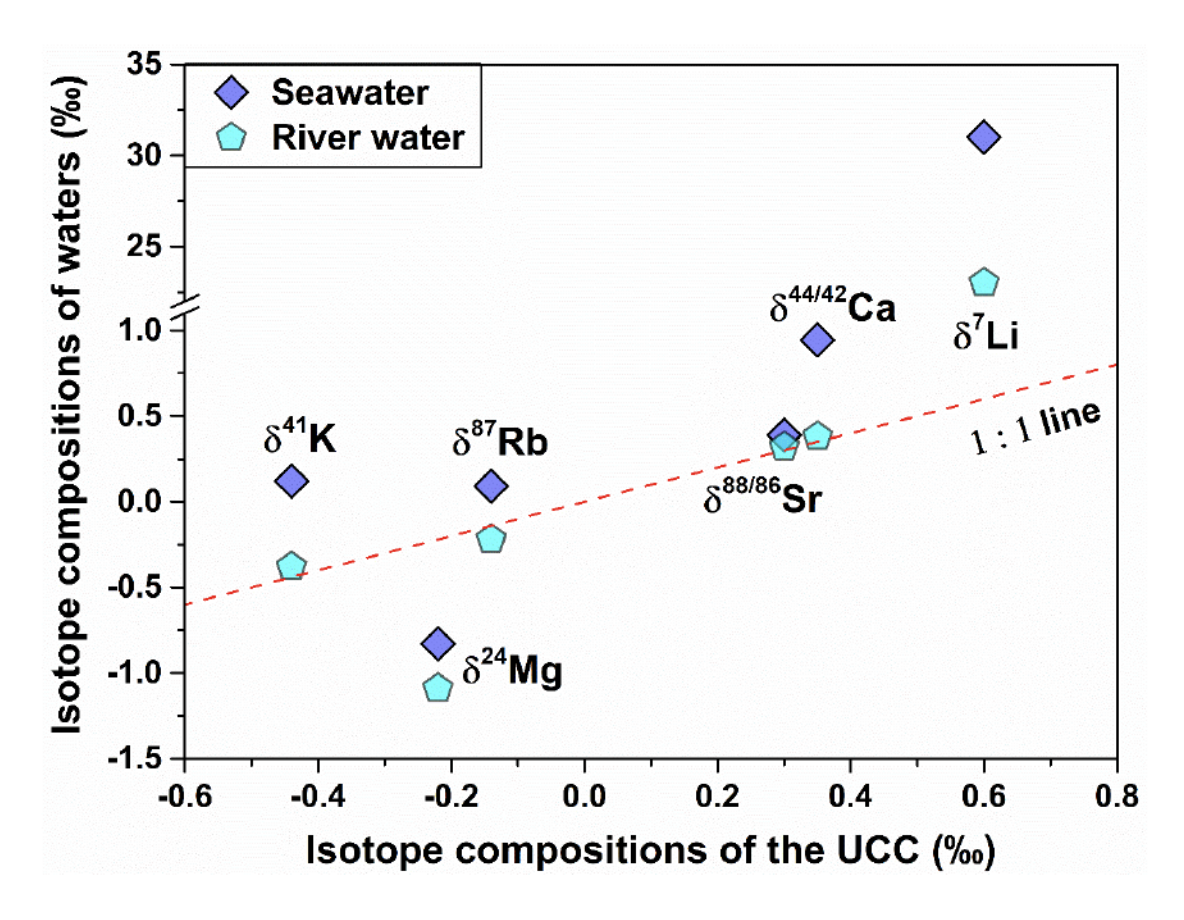












Tables

Click here to access/download **Supplementary material for online publication only**Supplementary appendix-Tables.xlsx

text

Click here to access/download **Supplementary material for online publication only**SI-EPSL-D-23-01439-R1.docx

Declaration of Interest Statement

All authors declare that we have no known competing financial interests or personal relationships that could have appeared to influence the work reported in this paper.